Optimization Methods for Equivalent Source Identification and Electromagnetic Model Creation based on Near-Field Measurements

D. Rinas, S. Niedzwiedz, J. Jia, S. Frei
Dortmund University of Technology
Dortmund, Germany
denis.rinas@tu-dortmund.de
simon.niedzwiedz@tu-dortmund.de
jin.jia@tu-dortmund.de
stephan.frei@tu-dortmund.de

Abstract— **The field emission from printed circuit boards (PCB) plays an important role in the electromagnetic compatibility of electronic systems. The established field measurement methods according to CISPR suffer from the need to use large anechoic chambers. Furthermore the measurement data cannot be used for modeling concerning the calculation of the overall fields radiated from e.g. a car. Other methods which try to identify an equivalent source distribution by near-field measurements do not require large anechoic chambers, but instead an electromagnetic inverse problem has to be solved. This often leads to an ill-posed equation system due to unavoidable errors in measurement data, long computation times, and finally inaccurate results. In this paper an approach to optimize the characterization method of printed circuit boards by near-field measurements is proposed. The radiation of a PCB is modeled with a set of elementary sources, resulting in the same field like the electronic system itself. The electromagnetic fields in a plane above the PCB are measured. Optimized time domain methods are applied in order to reduce measurement time, to receive phase information, and to correlate different measurement data sets. As the current distribution on a PCB mainly depends on the conductor paths, the distribution of characterizing equivalent sources can be chosen with respect to the trace routing. Amplitude and phase correlation of the equivalent sources along each current path are taken into account. The routing information can be extracted from mechanical CAD-data or is based on high-resolution near field scans. The approaches are integrated in the equivalent source identification process. The advantages of the new method are presented and discussed.**

I. INTRODUCTION

Electromagnetic Compatibility plays an important role in the development of electronic systems. Beside the radiating cable bundles PCBs can be significant sources for electromagnetic emissions.

Standardized component field measurement methods, like the ALSE antenna method provided e.g. in CISPR 25 [1] for evaluation of electro-magnetic emissions from automotive systems, suffer from the need of large and expensive anechoic chambers. Also a single field strength value is often not sufficient to characterize the EMI behavior of a complex system. Furthermore it is not possible to use the measurement data for behavioral simulation model creation. If accurate simulation models would be used, a statement about the radiating electromagnetic fields could be made in early development phases.

Basically the electro-magnetic emission can be distinguished in the emission of printed circuit boards with housing and the emission of the connecting cable bundles. Where in lower frequency range radiation from the bundles is dominant the importance of emission from PCBs grows with rising frequency.

To be able to determine the radiated far fields it is necessary to transfer the radiating PCB structure into an equivalent behavioral model with reduced complexity. Knowing the fields in an indefinitely extended plane above an object means, all information is available to calculate any field vector above this plane [2]. From theoretical point of view this would be sufficient to calculate the far fields. But there are several problems with such a direct approach. E.g. accuracy of measurements is limited and accuracy of far field calculation can be low. It is better to solve the inverse problem and thus to identify important properties of the test object by the measured field. This approach is discussed e.g. in [3], [4], [5] or [6].

Solution methods for the inverse problem, where equivalent elementary radiation sources are placed equally distributed and e.g. exciting dipole moments can be calculated by solving a linear equation system, are ill-posed due to the presence of measurement data errors. The measurements must have reliable amplitude and phase information in order to produce proper results. Because errors mainly occur in phase measurement [6] it is possible to retrieve the full complex field distribution data only from the knowledge of near-field amplitude data. This leads to an inverse problem, which is often tried to be solved using phase retrieval algorithms [7], [8]. Other approaches use optimization methods, in which spatial position, orientation, and magnitude of the sources is modified, until the field characteristics of the circuit board and its model agree in the reference plane [9]. These methods involve the problem of converging to local minima or lead very long computation

times for each model. One reason for the problems is the missing correlation of the approximating sources.

Methods to introduce physical correlations in the sources distribution can reduce the number of free source parameters and computation time. Additional possibilities of error correction are given. As the current distribution on printed circuit boards is mainly bounded to the trace geometry the spatial distribution of the sources can be limited. Furthermore amplitudes and phases of equivalent sources must be correlated to each other. Techniques for localization of current distribution are presented in [10]. Another approach investigated here is it to locate the traces by means of CAD-data of the board.

This paper presents a special method for estimating emissions from planar structures like printed circuit boards without vertical expansion in a frequency range up to 500 MHz. Therefore the electromagnetic near-field in a plane close to the test object is measured. For an equivalent model generation the approximating sources are distributed only along the traces. The parameters of the approximating sources are determined based on the field measurement data. Considering the correlation between the elementary sources the inverse problem is solved with optimization algorithms. The generated model enables different types of post-processing, e.g. far field estimations. The method can be combined with scan data of cable bundles, in order to determine the full system behavior and to create behavioral models for large system simulations.

To get fast the amplitude and phase information for the complete frequency range measurements are done in time domain, using a standard 4-channel digital oscilloscope, and subsequent FFT. The implemented data processing chain is presented in the following chapter.

II. TIME DOMAIN MEASUREMENTS WITH ADDITIONAL PHASE DETERMINATION FOR ACQUIRING COMPLETE NEAR FIELD INFORMATION

The measuring system shown in figure 1 can be subdivided into 3 functional parts – a preprocessing frontend including analog-to-digital-conversion to obtain data, the central digital signal-processing part including frequency domain transformation, and a post-processing algorithm for data correction and analysis as the data processing backend.

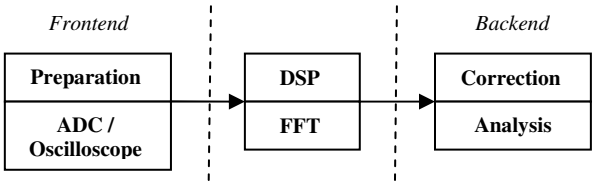

Figure 1. Time-domain measuring system

A. *Preprocessing techniques for increasing measuring dynamics*

In order to obtain data of higher precision it is important to increase first the quality of the underlying measurement raw data. This can be achieved by combining technological and methodical measures to a process chain as presented below (figure 2).

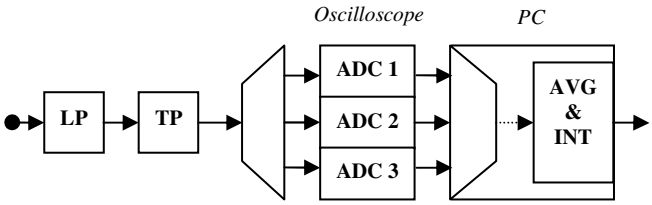

Figure 2. Preprocessing chain

The first and fundamental step in the process chain is the use of an analog low-noise low-pass filter, mainly to prevent alias effects. Additionally, this filter can also be used to mask upper frequency ranges that are not of interest or where known measurement system disturbances are present.

Additionally to the masking in the upper frequency range a masking of the lower frequencies from DC up to a threshold frequency can be implemented using a high-pass filter. This is done, for example, to analyze only certain harmonics instead of the fundamental with high amplitude.

However, besides this frequency band selection, a more important aspect is the increase of the amplitude dynamic range. The easiest way to lower the minimum level of detection is the use of an optional low-noise amplifier. But as the physical resolution of an oscilloscope's analog-to-digital-converters is fixed, i.e. less than 8-bit, the upper detection limit is simultaneously lowered leading to the dilemma to decide whether the larger or smaller signal parts are more important.

To overcome this dilemma one can use more than one oscilloscope channel – here 3 – to simultaneously measure the same signal with different vertical resolutions and later recombine the different channels' data to one signal with a than much higher resolution. Here the quantization characteristic of this multichannel-measuring that is not linear anymore, has to be taken into account. A fourth channel on the oscilloscope can be used as reference and trigger channel – for example to record the original stimulus signal of a device under test.

In order to benefit from the increased dynamic range it is additionally important to suppress white noise and to limit influences of non-stationary processes by averaging the results of repeated single measurements. This averaging can also be used to increase mathematically the dynamic range when using a data representation format having more bits than the original quantization – i.e. 32-bit instead of 16-bit – allowing a much finer quantization of the data values. Using interpolation techniques it is thereby possible to linearize or smooth the quantization characteristic of the multichannel-measuring.

At the end of this pre-processing chain a clearly enhanced time domain data base – optionally including the reference signal – is provided for the following Fourier-transformation, which will not be discussed here, and the post-processing.

B. *Post processing data correction methods*

The result of the Fourier-transformation is the complete complex near-field spectrum data, containing magnitude and phase information. As these data still contain the influences caused by the preprocessing chain it is necessary to apply post processing in order to correct and enhance the resulting data.

For removing those influences it is necessary to determine the complex transfer function of any equipment used within the measurement chain. These are used right after the domain-transformation to correct the resulting complex frequency domain data. Thereby the correct magnitude and phase information of the measured near-field data is restored.

It is necessary to determine the transfer function of each used measurement device first separately, and then calculate the transfer function of the whole chain afterwards or apply the single transfer functions successively. This approach allows a more detailed knowledge of the chain's influences and prevents that neutralizing effects within the chain are overseen. Furthermore it makes the structure of the chain easier adaptable to different use cases.

At the end the complete near-field information, including the correct magnitude and phase data, is available. It has to be taken into account that the phase data refers to a mathematically implicit cosine signal. If an optional reference signal is available, the difference between the two signals' phase data can be used.

C. *Advantages of time domain measurement system for source identification process*

A time domain measurement system as presented above has the advantage of obtaining the desired information in a considerable shorter time than a frequency domain measuring system. This allows near-field scans of large device with a very good spatial resolution in a very time- and thereby cost-efficient way. Combined with the techniques of the multichannel measurement and the averaging of multiple sweeps a very high dynamic range can be achieved.

So this provides a very efficient basis for creating maps of a PCB without having any CAD-data, especially when frequency selective maps for electromagnetic field components are of interest.

III. SOURCE IDENTIFICATION

For an electric current I_0 the magnetic vector potential $\vec{A}$ at observation point $\vec{r} = (x, y, z)$ is given by

$$\vec{A}.(\vec{r}) = \frac{\mu}{4\pi}\int_C \vec{I}_0(x_0, y_0, z_0)\frac{e^{-jk|\vec{r}|}}{|\vec{r}|}dl' \qquad (1)$$

where $|\vec{r}|$ is the distance to observation point, C is the path along the source and $\vec{r}_0 = (x_0, y_0, z_0)$ the source position. With (1) the magnetic field $\vec{H}$ can be calculated as

$$\vec{H} = \frac{1}{\mu} rot\vec{A}. \qquad (2)$$

To approximate the electromagnetic emission of a given planar structure a set of equally distributed electric dipoles can be used. As shown in figure 3 e.g. three orthogonal arranged dipoles each radiating a magnetic field given by

$$\begin{aligned}
H_x &= \frac{k_0}{4\pi}\left[\frac{z-z_0}{r}\left(\frac{1}{k_0 r}+j\right)\frac{1}{r}e^{-jk_0 r}I_{0y} - \frac{y-y_0}{r}\left(\frac{1}{k_0 r}+j\right)\frac{1}{r}e^{-jk_0 r}I_{0z}\right] \\
H_y &= \frac{k_0}{4\pi}\left[\frac{z_0-z}{r}\left(\frac{1}{k_0 r}+j\right)\frac{1}{r}e^{-jk_0 r}I_{0x} + \frac{x-x_0}{r}\left(\frac{1}{k_0 r}+j\right)\frac{1}{r}e^{-jk_0 r}I_{0z}\right] \\
H_z &= \frac{k_0}{4\pi}\left[\frac{y-y_0}{r}\left(\frac{1}{k_0 r}+j\right)\frac{1}{r}e^{-jk_0 r}I_{0x} - \frac{x-x_0}{r}\left(\frac{1}{k_0 r}+j\right)\frac{1}{r}e^{-jk_0 r}I_{0y}\right]
\end{aligned} \qquad (3)$$

where I_x, I_y and I_z are the dipole moments and H_x, H_y and H_z the magnetic field values in x, y and z direction [11].

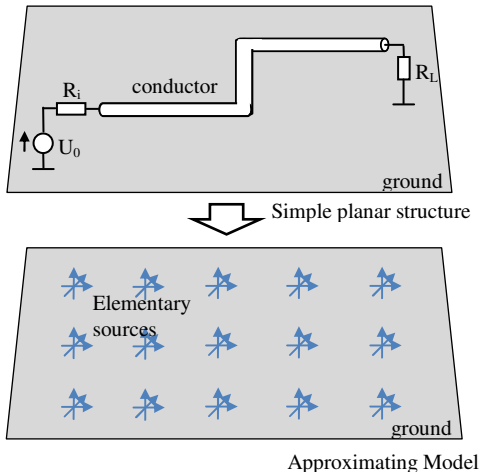

Figure 3. Simple planar structure (above) and approximating model with equally distributed sources (below)

Since the model is built with M dipole sets, the magnetic field is calculated as the sum of their contributions. To determine the dipole moments, a system of equations is set up to

$$I_0 = \psi^{-1}H \cdot \qquad (4)$$

Where ψ contains the wave vector k_0 and the remaining fixed geometric parameters for each dipole. H is the magnetic field, measured at N near field points in a plane above the planar structure. To get an accurate solution of the inverse problem the measurements must have reliable amplitude and phase information.

As the errors increase with rising frequency, mainly in phase measurement, the electromagnetic model can be created with amplitude data only, using the minimization functional

$$F = \left\|H^2 - B(H_0)\right\|^2 \cdot \qquad (5)$$

Where the B is a quadratic operator, with respect to real and imaginary parts of the magnetic field of the approximating sources H_0 and H are the measured field amplitudes [7]. Function (5) can be treated with the use of optimization algorithms. As described before, this approach often leads to long computation time and inaccurate solution [7][8].

IV. Methods for Source Identification Optimization

In this chapter methods to optimize the source identification process are introduced. Their benefit is the decrease of the number of free source parameters and the reduction of computation time. Furthermore they allow the use of error correction methods and increase accuracy of the results.

A. *Source distribution with compliance to the conducting paths geometries*

To improve the accuracy of a solution, mechanical CAD-data of the printed circuit board or location of the radiating conductors on the board from scan data can be integrated in the model creation process. This way the possible current paths are defined. With knowledge of the current paths the approximating dipoles no longer need to be equally distributed on the planar structure, but the source distribution can be precisely adapted to the physical board characteristics (figure 4).

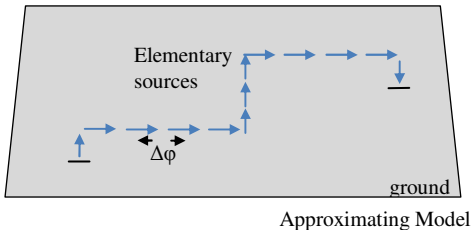

Figure 4. Drawingof the approximating model with sources along the current path

This leads to a considerable reduction of the number of elementary sources, the resulting reduction of computational cost and rise of model accuracy.

B. *Phase correlation of sources taking into account the conducting paths geometries*

Distribution dependences of the elementary sources adapted to the routing of the conductor are used to correlate phases of the dipoles. For a spatial distribution Δd the phase shift between two adjacent dipoles is set to

$$\Delta\varphi = \frac{2\pi}{\lambda}\Delta d \qquad (6)$$

as shown in figure 4. With adherence to (6) phase jumps between two sources greater and different from $\Delta\varphi$ are prevented and the model becomes more physically.

C. *Integration in source identification process*

In a first step, before calculation of free source parameters, the electric dipoles are arranged along the current paths. With that the geometric parameters for each dipole are specified. In a next step optimization methods are used to solve the inverse problem. Therefore the weighted minimization problem

$$F = (w_1, w_2)\cdot\begin{pmatrix}\|P\{H,H_0\}\|^2\\ \|A\{H,H_0\}\|^2\end{pmatrix} \qquad (7)$$

is considered. Where $P\{\}$ is the phase error and $A\{\}$ the amplitude error between H and H_0. w_1 and w_2 are the weights of phase and amplitude errors. This enables the algorithm to solve a complex or amplitude-only problem or to decrease relevance of phase in case of measurement errors.

For each step in evaluation of the minimization function the phase of only one source element $\varphi_{k,1}$ of each current path k is varied. With respect to (6) the other phases $\varphi_{k,m}$ are correlated with $\varphi_{k,1}$.

The process of source identification is shown in figure 5.

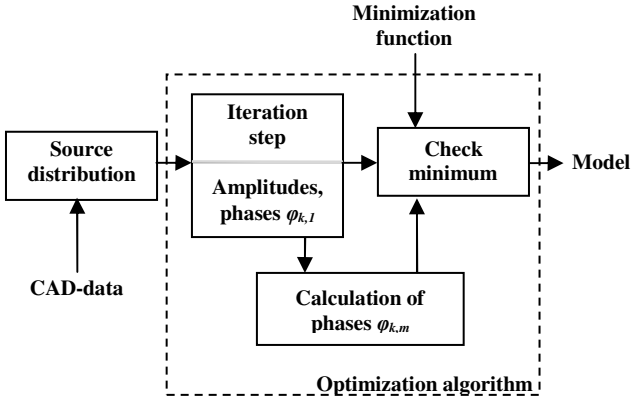

Figure 5. Process of source identification

V. Results

In the following section results are presented. Model creation process was tested with different configurations (figure 6) on the basis of measurements and Method of Moments (MoM) simulation data.

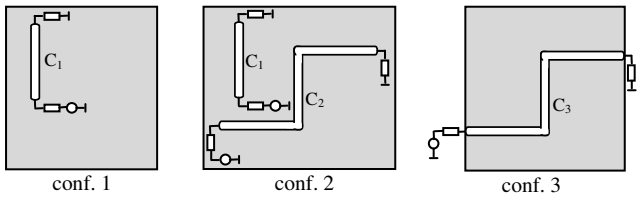

Figure 6. Test configurations; conf. 1 (left), conf. 2 (middle) and conf. 3 (right)

To show the improvement of the optimizations the weight of phase relevance w_1 in algorithm with respect to (7) is set to zero. Thus the source parameters are computed with amplitude-data only. Simulated Annealing is used as optimization method for finding the minimum of evaluation function. The

computation time for each discrete frequency is limited to 3 minutes.

A. *Increased measurement dynamic by multichannel measurement*

In figure 7 a comparison between a single-channel measurement and a multichannel measurement of 10 MHz rectangular pulse signal is shown. Clearly recognizable is the increased dynamic range in the multichannel measurement, thus providing a much better data base for source identification or the creation of frequency dependent field distributions of electronic devices.

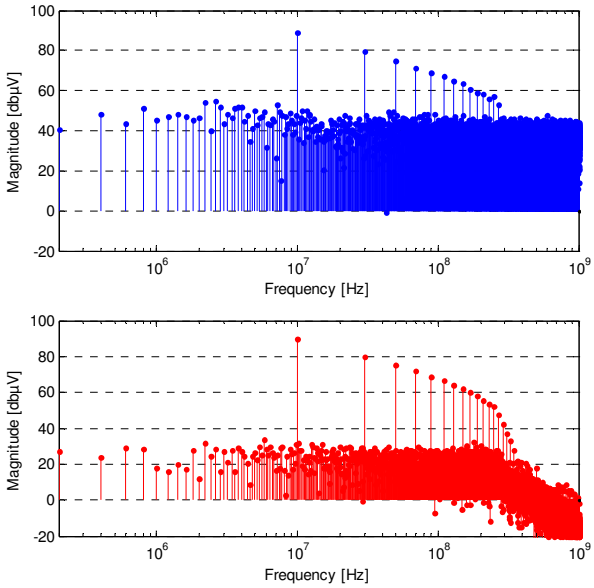

Figure 7. Comparison of single-channel measurement (above) and multichannel measurement (below)

B. *Source identification results*

1) *Configuration 1 – Simulation based results*

To show benefit of source location identification a simple planar structure (conf. 1), shown in figure 6 is analyzed. It consists of a 0.08 x 0.10 m plane and a conductor C_1 with length of 0.045 m. The source voltage is 1 Volt, with an internal resistance of 50 Ohm; termination is a 250 Ohm resistor. The magnetic field data is collected from MoM simulation in a height of 0.02 m over ground at 256 near field points.

In table I near field calculations of the electromagnetic model with equally distributed sources without phase correlation and the optimized model are shown and compared with a full field simulation (MoM). The frequency is set to 200 MHz. Figure 8 presents the magnetic fields of both models at a distance of 3 m in comparison with the full field simulation in a frequency range from 10 MHz to 1000 MHz.

As shown, the field approximation is much better when the distribution of sources is matched with the conductor path and the correlation of phases is considered.

TABLE I. MAGNETIC NEAR FIELDS OF BOTH MODELS IN COMPARISON WITH FULL FIELD SIMULATION AT 200 MHZ

Full field simulation		
	Equally distributed sources	Sources along current path with phase correlation
Approximating models		

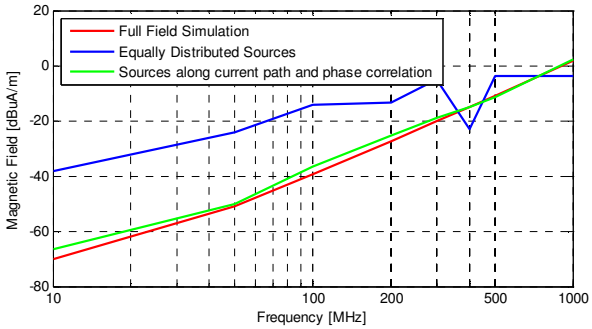

Figure 8. Magnetic field at distance of r = 3 m for both models in comparison with full field simulation

2) *Configuration 2 – Simulation based results*

The second example (conf. 2, figure 6) consists of a 0.16 x 0.12 m plane and two conductors. Conductor C_1 has a length of 0.045 m and C_2 has a length of 0.12 m. The source voltage is 1 Volt, with an internal resistance of 50 Ohm; termination of C_1 is a 250 Ohm resistance and a 100 µH inductance; termination of C_2 is a 1000 Ohm resistance. The magnetic field is collected from MoM simulation in a height of 0.02 m over ground at 256 near field points.

In table II near field calculations of the optimized model are shown and compared to a full wave simulation. The frequency is set to 200 MHz. Figure 9 presents the magnetic field of the model at a distance of 3 m in comparison with the full field simulation in a frequency range from 10 MHz to 1000 MHz.

TABLE II. MAGNETIC NEAR FIELD OF MODEL IN COMPARISON TO FULL FIELD SIMULATION AT 200 MHZ

Full Field Simulation	Sources along current path and phases correlation

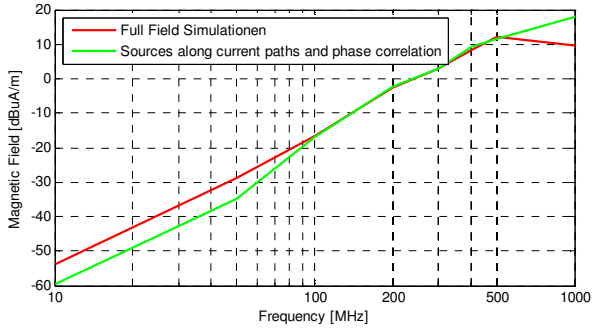

Figure 9. Magnetic field at distance of r = 3 m of the model in comparison with full field simulation

3) Configuration 3– Measurement based results

The analyses of the third planar structure (conf. 3, figure 6) is based on measurement data taken from the time domain measuring system presented in the previous chapters.

The configuration consists of a 0.16 x 0.1 m ground plane and a conductor C_3 with total length of 0.19 m. The internal resistance of the source is 50 Ohm; termination is 50 Ohm. The input is a pulsed signal, with a fundamental frequency of 4 MHz, rise and fall time of 10 ns, pulse/pause ratio of 1, and amplitude of 5 Volts (figure 10). The magnetic near field is measured in a plane 0.01 m over ground at 187 points.

Figure 11 shows the envelope of the magnetic field of the approximating model in comparison with the full field simulation of planar structure. The field is calculated at a distance of 3 m in a frequency range from 10 MHz to 200 MHz.

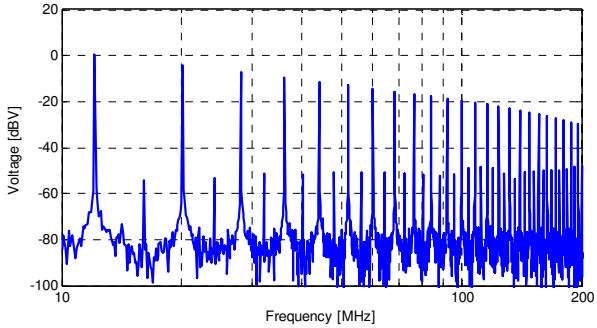

Figure 10. Pulsed input signal in frequency domain

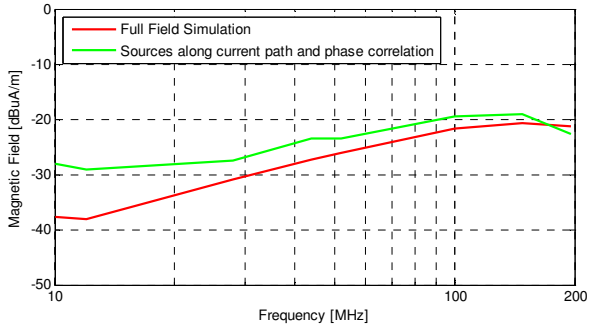

Figure 11. Magnetic field at distance of r = 3 m of the model in comparison with full field simulation

The results agree in a frequency range between 28 MHz and 200 MHz with a maximum error of 3 dB. The difference in lower frequencies might be due to measurement errors. Another reason could be the problem of finding a unique solution with the optimization algorithm, when the height of the scanning area decreases considerably in comparison to the wavelength.

VI. CONCLUSION

In this paper methods to optimize the process of equivalent sources identification are introduced. The sources distribution is chosen with respect to the routing on the circuit board. Correlations between phase data of sources along each conductor are considered and integrated in the computation process. The advantages of the approaches were shown on basis of magnetic near field data collected with a time domain measuring system and data based on Method of Moments simulations.

Further investigations in choice of height and resolution of the scanning area as well as the choice of the most suitable optimization algorithm for source parameter identification have to be done.

REFERENCES

[1] "CISPR 25 Ed.3: Vehicles, boats and internal combustion engines – Radio disturbance characteristics – Limits and methods of measurement for the protection of on-board receivers".

[2] Constantine A. Balanis, "Antenna Theory Analysis & Design", Wiley, 1996.

[3] Yolanda Vives Gilabert, "Modélisation des emissions rayonées de composants électroniques", Université de Rouen, 2007.

[4] D. Baudry, M. Kadi, Z. Riah, C. Arcambal, Y. Vives-Gilabert, A. Louis, B. Mazari, "Plane wave spectrum theory applied to near-field measurements for electromagnetic compatibility investigations", IET Science, Measurement and Technology, 15. June 2008.

[5] Tommaso Isernia, Giovanni Leone, Rocco Pierri, "Radiation Pattern Evaluation from Near-Field Intensities on Planes", IEEE Transaction on Antennas and Propagation, Vol. 44, No. 5, May 1996.

[6] Xin Tong, D.W.P. Thomas, A. Nothofer, P. Sewell, C. Christopoulos, "A Genetic Algorithm Based Method for Modeling Equivalent Emission Sources of Printed Circuits from Near-Field Measurements", APEMC Beijing, 2010.

[7] T. Isernia, G. Leone, R. Pierri, "Radiation pattern evaluation from near-field intensities on planes," IEEE Trans. Antennas Propogat., vol. 44, pp. 701–710, May 1996.

[8] R. Pierri, G. D'Elia, F. Soldovieri, "A two probes scanning phaseless near-field far-field transformation technique," IEEE Trans. Antennas Propogat., vol. 47, pp. 792–802, May 1999.

[9] Joan-Ramon Regué, Miquel Ribó, Josep-Maria Garell, Antonio Martin, "A Genetic Algorithm Based Method for Source Identification and Far-Field Radiated Emissions Prediction From Near-Field Measurements for PCB Characterization", IEEE Trans. On Electromagnetic Compatibility, vol. 43, No. 4, November 2001

[10] Qiang Chen, Jerdvisanop Chakarothai, Kunio Sawaya, "Estimation of Current Distribution by Near-Field Measurement", CEEM, China, 2009

[11] P. Wilson, "On Correlating TEM Cell and OATS Emission Measurements", IEEE Transactions on Electromagnetic Compatibility, 37, February 1995